Conformations in dioctyl substituted polyfluorene: A combined theoretical and experimental Raman scattering study

ARTICLE *in* THE JOURNAL OF CHEMICAL PHYSICS · MARCH 2007

Impact Factor: 2.95 · DOI: 10.1063/1.2434976 · Source: PubMed

3 AUTHORS:

Chris Volz
Indiana University Bloomington
2 PUBLICATIONS **60** CITATIONS
SEE PROFILE

Muhammad Mashhood Arif
Hasselt University
82 PUBLICATIONS **1,475** CITATIONS
SEE PROFILE

Suchismita Guha
University of Missouri
121 PUBLICATIONS **1,197** CITATIONS
SEE PROFILE

Conformations in dioctyl substituted polyfluorene: A combined theoretical and experimental Raman scattering study

C. Volz, M. Arif, and S. Guha[a)]
Department of Physics and Astronomy, University of Missouri, Columbia, Missouri 65211

(Received 25 September 2006; accepted 27 December 2006; published online 12 February 2007)

The structural properties of polyfluorenes (PF) are extremely sensitive to the choice of functionalizing side chains. Dioctyl substituted PF (PF8) adopts metastable structures that depend upon the thermal history and choice of solvents used in film forming conditions. We present a detailed study of the changes in the backbone and side chain morphology in PF8, induced by the various crystallographic phases, using Raman scattering techniques. The vibrational frequencies and intensities of fluorene oligomers are calculated using hybrid density-functional theory with a 3-21G* basis set. The alkyl side chains are modeled as limiting conformations: all *anti, anti-gauche-gauche*, and end *gauche* representations. The calculated vibrational spectra of single chain oligomers in conjunction with our experimental results demonstrate the β phase, which is known to originate in regions of enhanced chain planarity as a direct consequence of the alkyl side chain conformation. © *2007 American Institute of Physics*. [DOI: 10.1063/1.2434976]

I. INTRODUCTION

Blue-emitting conjugated polymers (CP) continue to be heavily researched mainly for display applications. Among these CPs, polyfluorenes (PF) are extremely attractive due to their high luminescence efficiency and facile processing characteristics allowing uniaxial chain orientation that result in linearly polarized emission.[1–4] A clear understanding between structural phase behavior and its impact on optical and transport properties in CPs is essential for new device technologies.

Solubilizing side chain substituents at the bridging carbon atom in PFs give rise to a rich array of mesomorphic behavior with the appearance of a nematic liquid crystalline (*n*-LC) phase.[4,5] Two chemically similar but structurally different side chain moieties have been heavily studied: poly[9,9′-bis(2-ethylhexyl) fluorene] (PF2/6) and poly[9,9′-(di-n-octyl) fluorene] (PF8). PF2/6 has a limited number of conformational isomers that form a fivefold helix (5/2 or 5/1).[6,7] These helices in turn self-organize into three-chain unit cells resulting in well ordered semicrystalline hexagonal phase with coherence lengths exceeding 50 nm.[8] Thus, the optical properties of PF2/6 are relatively insensitive to the exact crystallographic state, thermal history, or molecular weight.[9] PF8, on the other hand, has at least three conformational isomers that depend explicitly upon the torsional angle between the adjacent monomer, as shown by the arrow in Fig. 1(a). In addition to these isomers, structural studies of PF8 have identified many crystalline phases.[10,11]

There are many ambiguities regarding chain conformations and crystalline phases in PFs. Vibrational frequencies and intensities determined by Raman spectroscopy are strongly influenced by variations in the backbone as well as side chain conformations. Specifically in the PFs there is evidence of local inhomogeneities in the structural order that give rise to heuristic families of conformation isomers with, in sum, both segmental and wormlike disorder.[9] A prime example is the low energy emitting β chromophore in PF8, proposed to originate in regions of enhanced chain planarity, which reflects a surprising level of conformational order over short distances compared to other phases and conformations. This chromophore is identified in spectroscopic measurements as a separate long wavelength feature in both optical absorption and emission spectra.[4,5] Although this phase appears as a minority constituent it dominates the optical emission.[12,13] The application of Raman scattering is particularly useful in PFs for discerning the families of chain conformers and structural phases.

A recent modeling study by Chunwaschirasiri *et al.*[14] has identified three different conformational isomers in terms of the local polyfluorene backbone torsional angle: C_α, C_β, and C_γ that reflect the PF8 chain structure at very short length scales. The C_β, conventionally referred to as the β phase, is the more planar form with a torsional angle ~165° between adjacent monomer units; C_α and C_γ are associated with torsional angles of 135° and 155°, respectively. Structural studies have identified more than five different crystalline phases, with the *n*-LC phase being one of them which is induced at ~150 °C. Cooling from the *n*-LC phase yields the α and α' crystalline phases of PF8. In a recent x-ray diffraction (XRD) work, Chen *et al.* have identified the α' crystal polymorph as being similar to the α phase and, additionally, it is exceptionally well oriented with respect to the surface normal in both ultrathin and moderately thick films.[11] Other structural forms are specified as nematic glass or spin glass cast, and these phases may be obtained by thermal quenching from the *n*-LC state.[4,15]

In this paper we present a detailed Raman scattering study of the structural phase behavior in bulk PF8 under thermal treatment conditions. By explicit calculations of the

a)Author to whom correspondence should be addressed. Electronic mail: guhas@missouri.edu

Raman spectra of F8 oligomers, we further confirm the incompatibility of the C_β chromophore with the overall crystalline phase in PF8 as shown recently by Arif *et al.*[16] Comparison of the calculated Raman spectra from F8 oligomers including varying side chain conformations with the experimental results further elucidate the interdependence of the backbone and side chain morphology.

Side chain conformation as a function of the crystalline phase in PF8 is probed by studying the low frequency region (100–800 cm^{-1}) of the Raman spectrum. Our experimental data along with model calculations of F8 monomers with limited side chain conformations, when compared with the known structure of *n*-alkanes give insight into the ordering of octyl side chains in the polymer. Conformations in *n*-alkane chains using vibrational spectroscopy have been heavily studied in the past three decades.[17–19] An accepted picture in the *n*-alkanes upon heating is that the crystallization goes through the formation of seeds consisting of weakly bundled segments of transplanar chains with short chain segments.[20] Raman and infrared spectroscopy (IR) have been particularly useful for identifying nonplanar defects, such as *gauche* defects in alkanes.[21,22] In perfect transplanar *n*-alkanes the low frequency Raman spectrum shows intense bands that arise from a longitudinal accordion motion (LAM) of the chain skeleton and its overtones.[23] In nonadecane, for example, LAM1 and LAM3 modes appear at 125 and 342 cm^{-1}, respectively.[17]

This paper is organized as follows; Sec. II describes our experimental and theoretical methodologies. In Secs. III and V, we present our theoretical and experimental results, respectively. Sec. V is a discussion of our results, followed by a summary in Sec. VI.

II. METHODOLOGY

A. Experimental details

The PF8 sample was obtained from American dye Source (BE-129) and dissolved in solvents such as *p*-xylene or toluene and then dried. The starting solutions were prepared with 10 mg of PF8 in 1 ml of the solvent (*p*-xylene or toluene). Bulk samples were obtained by repeatedly adding solution, as it dried, into small channels. A large thick residue eventually formed and pieces of the PF8 were then used for the Raman measurements. For aging studies, thin films were cast on sapphire substrates using the above PF8 toluene-based solution.

The absorption measurements were carried out using a Shimadzu UV-visible spectrophotometer. The Raman spectra were collected by an Invia Renishaw spectrometer attached to a confocal microscope with a ×50 long objective and a 785 nm line of a diode laser as the excitation wavelength. Typical laser power was a few milliwatts on the sample. The samples were affixed to a stainless steel sample holder of a Linkam LTS350 microscope hot-cold stage for thermal cycling studies. For Raman measurements from crystalline fluorene, we used an unpolarized macro-geometry (SPEX 0.85 m double spectrometer) equipped with a liquid N_2 cooled charge coupled device array detector and 514.5 nm line as the excitation line. This was done so as to better compare the theoretical unpolarized Raman intensities with experiment.

B. Computation

All theoretical computations of fluorene oligomers were performed with hybrid density-functional theory in the GAUSSIAN03 program.[24] We employed the B3LYP (Becke's three parameter hybrid) functional to perform geometry optimization and calculations of force constants, dipole moments, and polarizability derivatives combined with the polarized 3-21G* basis set.[25] Other basis sets such as the 6-31G or 6-311G yield comparable frequencies but often give unsatisfactory Raman intensities.[26] Recently it has been shown that compact basis sets such as Z2PolX and Z3PolX with B3LYP yield accurate Raman frequencies and intensities in organic molecules.[27]

The Raman spectrum calculations are performed in two steps; first the force constant matrix is evaluated and then the eigenvalue equation is solved to obtain the eigenvalues and eigenvectors. The Raman scattering activities are proportional to the polarizability derivatives taken with respect to the Cartesian coordinates. For a system of N atoms interacting via harmonic forces, the normal mode frequencies ω_f and amplitudes $\chi(f)$ of mode f, where $f=1,\ldots,3N$ labels the normal modes, are determined by a $3N\times 3N$ matrix eigenvalue equation,

$$(\Phi - \omega_f^2 \mathbf{M})\chi(f) = 0, \tag{1}$$

where Φ is the harmonic force constant matrix and $\mathbf{M}$ is the mass matrix. Both the force constant and mass matrices are symmetric.

The Raman intensities are theoretically obtained from the first derivatives of the polarizability with respect to the nuclear coordinates. In the harmonic approximation, the intensity of off-resonance first-order Stokes scattering is given by[28]

$$I_{\eta\eta'} \propto \omega_L \omega_S^3 \sum_{f=1}^{3N} \frac{\langle n(\omega_f)+1\rangle}{\omega_f} \left| \sum_{\alpha\beta} \eta_\alpha \eta_\beta P_{\alpha\beta,f} \right|^2 \delta(\omega - \omega_f), \tag{2}$$

where ω_L and ω_S are the incident and scattered light frequencies; $\omega=\omega_L-\omega_S$ is the Raman shift. η and η' are unit vectors along the incident and scattered polarization direction, respectively; $\langle n(\omega_f)\rangle \equiv [\exp(\beta\hbar\omega_f)-1]^{-1}$ is the thermal average occupation number of mode f at temperature $T=(k_B\beta)^{-1}$. $P_{\alpha\beta,f}$ is the derivative of the electronic polarizability tensor with respect to the normal coordinate of mode f; α and β are Cartesian coordinates. The Gaussian program calculates the Raman activities, which are given by the square of the polarizabity tensor in Eq. (2) from static polarizabilities.[29] To obtain the individual Raman intensities, the Raman activities were divided by the mode frequencies and multiplied by the thermal average occupation number at 300 K and the incident laser line (785 nm for PF8 and 514.5 nm for fluorene, respectively) using Eq. (2). The Raman intensities are further normalized to the C–C intraring

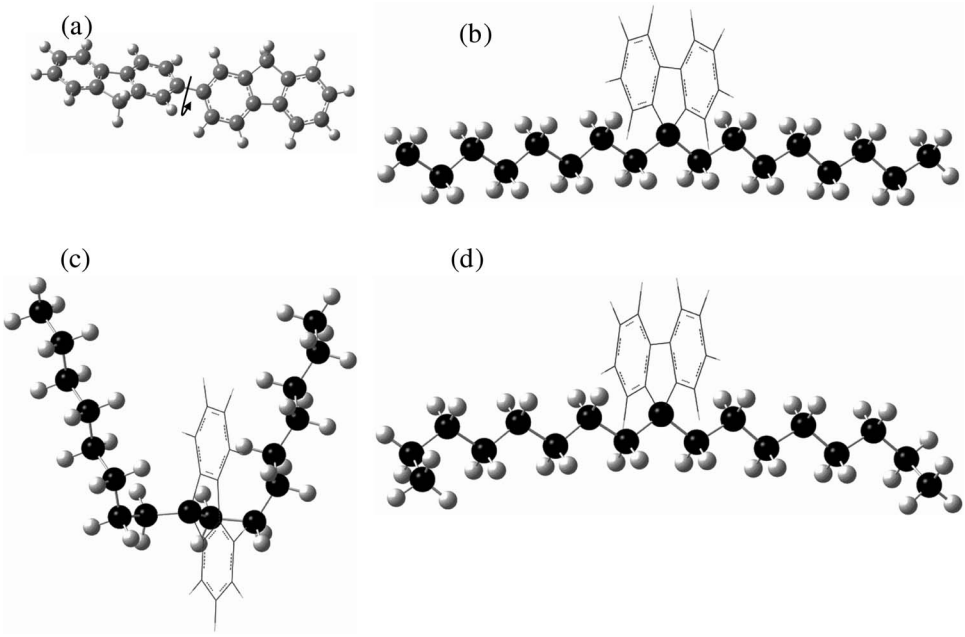

FIG. 1. Sketch of a (a) fluorene dimer and fluorene monomer with (b) *aaa*, (c) *agg*, and (d) *aag* side chain conformations.

stretch mode at 1600 cm^{-1} and have been broadened with a Lorentzian line shape of full width at half maximum (FWHM) of 10 cm^{-1}. All calculated frequencies reported here are unscaled.

The Raman frequencies were calculated from fluorene monomers for limiting conformations of the *n*-octyl side chains (see Fig. 1): all *anti* (*aaa*), *anti-gauche-gauche* (*agg*), and end *gauche* (*aag*) side chain conformations. Vibrational frequencies of a fluorene dimer, trimer and tetramer with no side chain substitution were calculated by varying the torsional angle between the monomers as test cases for conformational isomers of PF8.

III. THEORETICAL RESULTS

A. Fluorene: Comparison of theory with experiment

Figure 2 compares our calculated Raman frequencies and intensities of a fluorene monomer with experiment. Only the Raman peaks above 400 cm^{-1} and intensities greater than ~7 $Å^4$/amu are shown in the figure. The experimental measurements are from fluorene crystals measured with the 514.5 nm excitation line using an unpolarized 45° scattering macro-geometry. Unfortunately, the micro-Raman system equipped with a 785 nm excitation line used for all our PF8 measurements has a perfect backscattering geometry. As a result the Raman intensities are extremely sensitive to the orientation of the fluorene crystallites. To compare our calculated unpolarized Raman intensities, it is best to compare with a 45° scattering geometry. For the calculated fluorene spectrum we use ω_L as the 514.5 nm line in Eq. (2). We note that the Raman spectra of PF8 in this work have all been measured and calculated with the 785 nm line as the excitation source.

The calculated Raman frequencies are slightly higher than the experimental ones, and are in good agreement with previous theoretical work.[30] A small disagreement is inevitable since the calculations are for an isolated molecule and the experiment is in the solid phase. We also note that the theoretical intensities are systematically lower than experiment. This is attributed to resonance effects in the measurements due to excitation with the 514.5 nm line. A description of the backbone Raman modes is tabulated in Table I.

The peak positions denoted in Fig. 2 are the experimental values. The peak at 419 cm^{-1} corresponds to a ring torsion mode of the two phenyl rings in the monomer. The second peak at 744 cm^{-1} is a ring breathing mode which is also seen in biphenyl at a slightly higher frequency.[31] The Raman peak at 844 cm^{-1} is a combination of ring distortion of the phenyl rings and a C–C stretch of the bridging carbon. The 1020 cm^{-1} peak is mainly a C–H bending mode, which occurs in the plane of the phenyl rings and has a residual effect which distorts the phenyl rings. The 1234 cm^{-1} peak, the second strongest peak in the calculations, is mainly a C–C inter-ring stretch along with a C–H bend motion result-

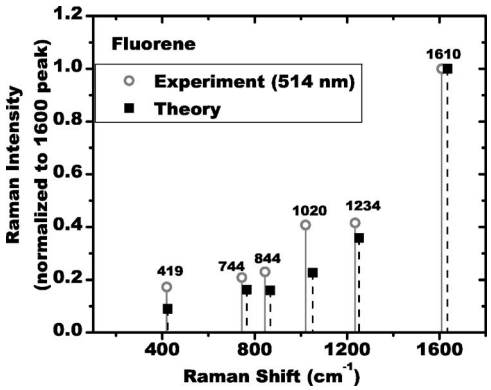

FIG. 2. Experimental (solid line) and calculated (dashed line) normalized Raman intensities and frequencies of fluorene. The intensity of the 1610 cm^{-1} peak has been set equal to unity.

TABLE I. Calculated and experimental Raman frequencies of the vibrational backbone modes. The first two columns are the calculated Raman frequencies of a fluorene monomer and tetramer in the α configuration, respectively. The third and fourth columns are the experimental data of fluorene crystal and PF8 at RT, respectively.

Raman frequencies (cm^{-1})				
Calculated		Experimental		Description
Monomer	Tetramer (α)	Fluorene	PF8 (as is)	
423	427	419	417	Ring torsion (inter-ring)
	449		480	Ring torsion (out of plane); C–H bend
765	780	744	735	Ring breathing
867	865	844	865	C–C stretch (bridging C)
1051		1020		C–H bend (in plane)
1135	1137/1143	1150	1135	C–H bend (in plane); ring distortion
1251	1253	1234	1232	C–C stretch (inter-ring)
	1244		1257	C–H bend (in plane)
	1302		1280/1302	C–C stretch (between monomers)
	1368		1350	C–C rock (between monomers)
1635	1628	1610	1605	C–C stretch (intraring)

ing in a minor ring distortion. The strongest peak is the 1610 cm^{-1} peak, which arises from an intraring C–C stretch type motion.

B. Conformational isomers: Oligomers with varying torsional angle

Figure 3 shows our calculated Raman spectra for an optimized dimer, trimer, and a tetramer. The inset shows the optimized structure of a tetramer. The optimized structures have a torsional angle of 138° between adjacent monomers and thus represent the C_α conformer. The Raman peaks in the 1140 cm^{-1} region originate from a C–H in-plane bend motion along with a ring distortion. In the planar (β) conformation or in the monomer there is mainly one Raman band around ~1135 cm^{-1} that originates from the terminal phenyl rings. In nonplanar conformations (α or γ), the motion splits as two or more vibrations originating from monomer units about the center of symmetry of the molecule as well as from the end rings. With increasing chain length, for the same conformation, the 1143 cm^{-1} is the dominant peak as seen in Fig. 3. The strong Raman peak at 1304 cm^{-1}, which corresponds to a C–C stretch mode between adjacent monomers, is very sensitive to the torsional angle. The frequency position of this peak thus serves as a good indicator of the conformational isomers. The 1320 cm^{-1} peak which is again a combination of a C–H bend between the monomer units and a C–C stretch motion within the monomer decreases in intensity and shifts to higher frequencies with increasing chain length. For the tetramer the 1320 cm^{-1} peak almost disappears and only the 1370 cm^{-1} peak, which is the true backbone C–C stretch motion within the monomer, is seen.

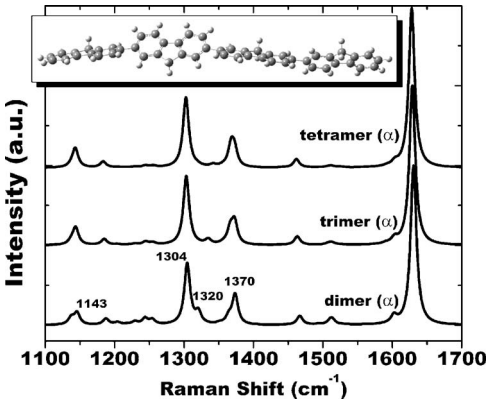

FIG. 3. Calculated Raman spectra of a fluorene dimer, trimer, and tetramer for the C_α conformation. The inset shows an optimized structure of the tetramer.

The Raman spectra of the oligomers were calculated by varying the torsional angles between adjacent units so as to mimic the C_α, C_γ and C_β conformers. The β conformers were simulated by fixing the torsional angle to 180°. For the trimer, we simulated a special case ($\alpha+\beta$) where one of the torsional angles was fixed at 180° and the other is the optimized angle at 138°. For the tetramer we simulated two intermediate cases: γ_1 where the first angle between the monomers was held at 180° and the other three optimized (at 138°) and γ_2 where the first two angles were held at 180° and the other two optimized. The latter yields similar results to the β conformer. The calculated spectra in the 1300 cm^{-1} region are plotted in Fig. 4 for the various conformers. The C–C stretch mode between adjacent monomers is strongly impacted by the torsional angle. This peak softens by almost 16 cm^{-1} for C_β compared to C_α. For intermediate situations two peaks are observed, one at 1304 cm^{-1} from the optimized units and a second peak at 1288 cm^{-1} from the C_β units. Side chain attachment to the bridging carbon atom reduces the symmetry of oligomers resulting in a splitting of peaks in this region. The experimental situation is thus complicated due to varying torsional angles and side chain conformations.

Next we simulated the Raman spectra of fluorene monomers with varying side chain conformations. Unfortunately, van der Waals interactions cannot be accurately incorporated at the B3LP level; without these interactions there are inaccuracies in the vibrational spectra of side chain substituted

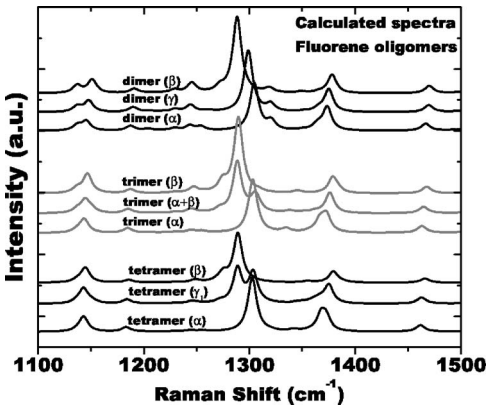

FIG. 4. Calculated Raman spectra of a fluorene dimer, trimer, and a tetramer for varying torsional angles. The notation for α, β, and γ conformers is described in the text.

oligomers. For this reason we limit ourselves to only monomers with various side chain conformations (see Fig. 1).

C. Monomers with varying side chain conformations

Different conformations of alkane chains show variations in the Raman peak positions and intensities mainly in the low frequency region and in the 800–1000 cm^{-1} region. The latter arises from end *gauche* defects and other nonplanar conformations. Figure 5 shows the 100–1000 cm^{-1} frequency region for three different chain conformations attached to the bridging carbon of a fluorene monomer: *aaa*, *aag*, and *agg*. Only the *aaa* conformation shows the LAM modes; the strongest peak being LAM1 at 133 cm^{-1} (shown by an arrow) and LAM3 at 370 cm^{-1}. These peaks are absent with the presence of *gauche* defects. The 420 and the 737 cm^{-1} Raman peaks are from fluorene itself as discussed in Sec. III A. The 200 cm^{-1} band in the *aaa* conformation is an out of plane motion of the two phenyl rings. This motion diminishes in the *aag* and *agg*, and only the rocking motion of H atoms on C1–C3 atoms of the side chain at ~223 cm^{-1} remain prominent. (Note: C1 position corresponds to the carbon atom closest to the bridging carbon atom.) The 333 cm^{-1} peak that appears in all three side chain conformations is an out of plane ring torsion motion. With the presence of

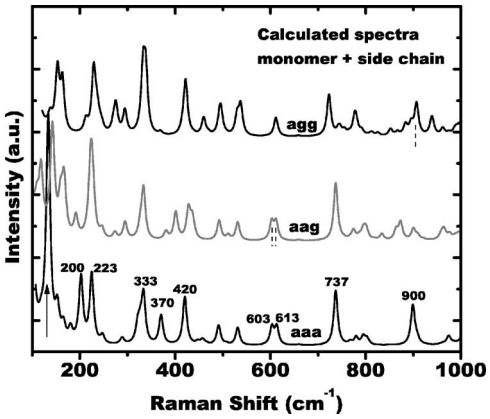

FIG. 5. Calculated Raman spectra of a fluorene monomer with dioctyl side chains attached to the bridging carbon atom. The simulations are for *aaa*-, *aag*-, and *agg*-type conformations.

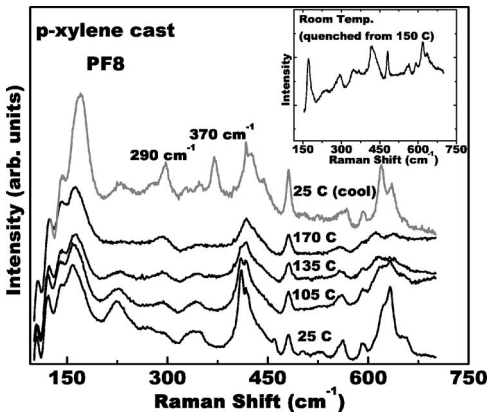

FIG. 6. Experimental Raman spectra of bulk PF8 cast from *p*-xylene at selected temperatures during the heating cycle. The top spectrum was measured at RT upon cooling the sample from 170 °C. The inset shows the Raman spectrum of another *p*-xylene cast PF8 sample at RT that was quenched from 150 °C.

gauche defects, a CH_2 wag motion at 338 cm^{-1} on C1 and C2 is the dominant one. The 600 cm^{-1} region also shows distinct differences that can be directly correlated to the presence of the β chromophore. The *aaa* and *aag* show a splitting as indicated by the dashed line. The lower frequency at 603 cm^{-1} corresponds to a stretching motion of the bridging C atom connected to the first CH_2 group. The higher frequency at 613 cm^{-1} peak is a wagging motion of hydrogens on the first CH_2 group from the bridging carbon and also involves a torsion of the phenyl rings. The *agg* conformation is characterized by only the latter peak.

Another notable feature in Fig. 5 is the 900 cm^{-1} region. In the *aaa* conformation there is a single peak at 900 cm^{-1} which corresponds to a C–C stretch motion of C6 and C7 carbons of the alkyl chain. With the presence of *gauche* defects this C–C stretch motion is coupled with other neighboring CH_2 rocking type modes. Experimentally there are significant changes in this region as a function of thermal cycling, which can be correlated to the side chain morphology.

IV. EXPERIMENTAL RESULTS

The changes in the Raman spectrum of PF8 as a function of thermal cycling reflect changes in both the backbone and side chain conformations. Previous works on Raman scattering of PF8 as a function of temperature mainly focused on the backbone Raman modes.[32,33] The low frequency Raman peaks (100–700 cm^{-1}) are extremely sensitive to both the composition and ordering of side chains. Figure 6 shows the low frequency region of PF8 cast from *p*-xylene at selected temperatures during the heating cycle. The top spectrum was taken after cooling the sample at room temperature (RT). The ring torsion mode at 480 cm^{-1} peak is seen in all PFs with different side group substitutions and is almost temperature independent. The 220 cm^{-1} peak observed in the as-is polymer corresponds to the disordered longitudinal accordion motion (D-LAM) in *n*-alkanes, which results from the motion of conformationally disordered alkyl chains having short *trans*-planar CH_2 sequences. The broad peak centered around 340 cm^{-1} arises from *gauche* defects in the as-is polymer,

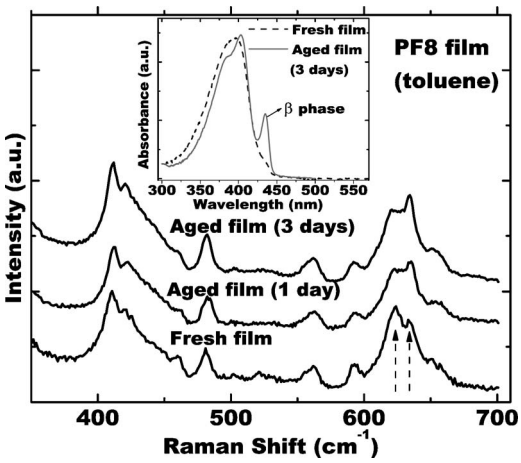

FIG. 7. Raman spectra of a PF8 film cast from toluene. The films were aged in toluene vapor. The inset shows the absorption spectra from the same films.

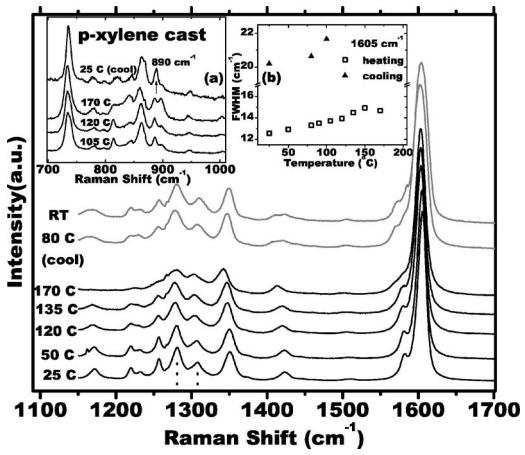

FIG. 8. Raman spectra of *p*-xylene cast PF8 sample at selected temperatures. The top two spectra were measured during the cooling cycle. Inset (a) shows the Raman spectra between 700 and 1000 cm^{-1} at selected temperatures. Inset (b) shows the full width at half maximum of the 1605 cm^{-1} Raman peak both during the heating and cooling cycles.

and it disappears at temperatures upward of 135 °C.

Upon annealing, two new peaks appear at 290 and 370 cm^{-1}. The latter corresponds to LAM3 motion of the alkyl chain, representing a high fraction of all *anti* side chain conformations. Additionally, there is an enhancement of the LAM1 mode (150 cm^{-1}) upon annealing. These changes upon annealing can be interpreted both in terms of the conformational isomers and the overall crystalline phase, as discussed in Sec. V. The inset shows a RT spectrum of the PF8 sample that was quenched from 150 °C. Thermal quenching suppresses side chain crystallization as evident from the lack of the LAM3 mode.

The relative ratio of the Raman intensities of the peaks at 620 and 633 cm^{-1} track the presence of the β phase. This is clearly seen in Fig. 7 which is from a PF8 film cast from toluene, where simultaneous optical absorption and Raman spectra were measured. Note that the calculated frequencies for the monomer in this region (Fig. 5) slightly soften. Fresh spin cast PF8 film exhibits only a small fraction of the β phase, as evident from the absorption spectrum (inset, Fig. 7). Correspondingly, the 620 cm^{-1} Raman peak is higher in intensity. Aging PF8 in toluene vapor is known to enhance the fraction of C_β chromophore.[34] This is clearly seen as a redshift in the absorption spectrum with the appearance of the 433 nm peak. The Raman spectrum shows an enhancement of the 633 cm^{-1} peak with the evolution of the β phase. In light of this, the *p*-xylene sample (Fig. 6) has a large fraction of the β phase at the onset. Upon thermal cycling, the C_β conformers diminish as evident from the increasing intensity of the 620 cm^{-1} Raman peak. The C_β conformer itself undergoes a reversible order-disorder transition near 80 °C,[4] and upon thermal cycling it most probably undergoes a transformation where the local intra-chain structure is a mixture of C_α and C_β type isomers.

The high frequency region between 1100 and 1700 cm^{-1} is shown in Fig. 8. The Raman frequencies in the 1200–1350 cm^{-1} region are mainly from a backbone C–C stretch motion; the higher frequency peak at 1342 cm^{-1} is the C–C stretch mode from within the monomer unit. The C–C stretch mode between adjacent monomers splits into two bands, appearing at 1280 and 1308 cm^{-1}, and is shown by dotted lines. The 1257 cm^{-1} corresponds to a C–H bend type motion and its intensity depends upon the backbone torsional angle.[16] The weak peak at 1420 cm^{-1} corresponds to a combined C–H bend and C–C stretch between adjacent monomers. The C–C intraring stretch mode at 1600 cm^{-1} broadens significantly when the polymer goes through crystallization, as shown in inset (b). Inset (a) of Fig. 8 shows the changes in the 900 cm^{-1} region upon annealing, which can be explicitly correlated to side chain conformations. This is discussed in detail in the following section.

V. DISCUSSION

The complexity in deciphering the Raman spectra of PF8 arises from the fact that the polymer must be simultaneously assessed in terms of its crystallographic phase and the distribution of conformational isomers, and the two are interdependent. Gas phase molecular mechanics calculations by Chunwaschirasiri *et al.* show that the C_β conformer is stabilized when the alkyl chains adopt an *agg* conformation.[14] In other words, a planar backbone conformation of PF8 requires the presence of *gauche* defects in the alkane chains. Although these calculations ignore three-dimensional packing it reveals some basic attributes of the local intrachain structure.

Both solvent and thermal history play a role in determining the crystalline phase in PF8. In a recent work that combines XRD, Raman scattering, and photoluminescence excitation, it is seen that PF8 samples cast from various solvents appear in a metastable structure at RT. The progression towards the well ordered α crystal phase is extremely variable; PF8 cast from *p*-xylene is marked by an intermediate *M* phase at RT when cooled quickly.[35] This phase is intermediate between the α and α' and presumably corresponds to the C_γ type family. In order to compare our theoretical results with experiment we divide the Raman spectra into three regions: (a) 100–700 cm^{-1}, (b) 700–1200 cm^{-1}, and (c) 1200–1700 cm^{-1}.

A. Low frequency region (100–700 cm^{-1})

This region is mainly characterized by Raman bands that originate from the alkyl side chains. The *aaa* conformation is characterized by strong LAM1 and LAM3 peaks at 150 and 370 cm^{-1}, respectively (as seen in Fig. 5). The 370 cm^{-1} peak is absent with the presence of *gauche* defects. The *p*-xylene sample has a high fraction of C_β chromophores at the onset implying a high fraction of *agg*-type side chain conformation. Upon thermal cycling from the *n*-LC phase, the Raman band at 370 cm^{-1} is clearly seen. Additionally, there is an enhancement of the 150 cm^{-1} peak. These changes are indicative of a large fraction of all *anti* side chain conformation. This correlates with the overall crystalline phase where the sample is in the so called *M* state, which precludes the presence of β conformers.[35] The diminishing intensity of the 340 cm^{-1} peak with increasing temperature also suggests a decrease in the *gauche* defects. The quenched sample (Fig. 6, inset) does not show any signature of the LAM3 mode, suggesting the suppression of polymer crystallization. The origin of the 290 cm^{-1} peak in our experiment is still not clearly understood and is under investigation.

The 600 cm^{-1} region, which tracks the β phase is seen as a split peak in the *aaa*- and *aag*-type conformations (Fig. 5). The *agg* conformation is characterized by only the higher frequency band. These features correlate with our experimental results very well. Since the polymer has a mixture of various side chain conformers both peaks in the 600 cm^{-1} region are observed for all crystalline phases. It is mainly the ratio of the relative intensities of these two peaks that changes as the polymer goes through various changes in its conformation. At the onset the 633 cm^{-1} peak is stronger than the 620 cm^{-1} peak, consistent with a higher fraction of *agg*-type conformer which is a prerequisite for the β phase. Upon annealing, (when PF8 is in the *M* phase) the 633 cm^{-1} peak substantially decreases in intensity indicating a loss in the *agg*-type chain conformers. One observes the same trend in a toluene-based PF8 film, as shown in Fig. 7. The observation here is consistent with the idea that the β phase is itself metastable and incompatible with the crystalline PF8 phases.

B. Medium frequency region (700–1100 cm^{-1})

The 735 cm^{-1} Raman peak experimentally observed in PF8 corresponds to the 747 cm^{-1} of a biphenyl with A_1 symmetry, providing sensitivity of this vibration to the planarity of the ground state.[36] With the presence of C_β chromophores, there is a splitting of this peak which is seen at RT before thermal cycling [not shown in the inset of Fig. 8(a)]. Our calculations of the mixed phase oligomers (γ_1 and γ_2 tetramer) show that there is a neighboring infrared active mode that becomes Raman active. With the presence of C_β chromophores since the symmetry of the molecule is lowered, most probably the IR active mode is seen in the Raman spectrum. Experimentally this doublet evolves as a single peak upon thermal cycling, again suggesting a loss of the β phase.

The calculated Raman spectra of fluorene monomers with different side chain conformations show significant changes in the 900 cm^{-1} region (see Fig. 5). In the *aaa*-type monomer there is only one peak in this region; the presence of *gauche* defects introduces other CH_2 rocking type modes. These features corroborate our experimental data [Fig. 8(a)]. Upon annealing, the 900 cm^{-1} peak gains intensity and is the predominant one. This observation is again consistent with a higher fraction of *aaa*-type side chains in the crystalline phase of PF8.

C. High frequency region (1100–1700 cm^{-1})

The 1200 cm^{-1} region is very sensitive to the backbone torsion angles and thus changes in the Raman spectrum in this region represent the conformational isomers. The C–C stretch mode between monomers splits into two peaks at 1280 and 1308 cm^{-1} in PF8. The peak position of the latter, in particular, tracks the changes in the C_β chromophore upon annealing. The 1308 cm^{-1} peak softens by almost 16 cm^{-1} for C_β in comparison to C_α as seen in Fig. 4. Experimentally one observes an enhancement in the 1308 cm^{-1} peak position at ~130 °C suggesting a transformation to C_α and C_γ conformers. Further, the intensity of the 1257 cm^{-1} peak is highly sensitive to temperature and tracks the transformation of C_β chromophore. By tracking the frequency position of the 1308 cm^{-1} peak and the intensity of the 1257 cm^{-1}, we find that the C_β chromophores decrease substantially upon heating the polymer above 130 °C. In this phase there is a higher fraction of the C_α chromophores. Upon cooling the polymer back to RT from *n*-LC there is a higher fraction of the C_γ isomers. The changes in the 1300 cm^{-1} region have been discussed in detail in Ref. 16.

The 1600 cm^{-1} broadens significantly upon crystallization of PF8 [Fig. 8(b)]. At the onset the FWHM of the peak is 12 cm^{-1} which in the annealed sample goes up to 20 cm^{-1}. Our gas phase calculation unfortunately does not track the FWHM as a function of the torsional angle, suggesting that the broadening observed in the experiment is a consequence of the changing intermolecular and intramolecular force constants when the polymer is in the so called *M* phase.

VI. SUMMARY

In this work we have shown a one-to-one correlation between changes in the vibrational spectra of PF8 upon thermal annealing with changes in the backbone and side chain conformations. The polymer is characterized by many crystalline phases as well as a distribution of conformational isomers. The Raman peak positions and intensities are strongly influenced by the local chain planarity and side chain conformations. The side chain conformation is best understood by tracking the Raman spectra in the low frequency region. At the onset the as-is PF8 sample is characterized by a high fraction of C_β conformers, which dictates the side chain conformation to be more of an *agg* type. Cooling *p*-xylene-based PF8 from its *n*-LC phase to RT results in a crystalline state that is intermediate to α and α' crystal forms. In this phase our Raman scattering data suggests a

higher fraction of the *aaa*-type alkyl side chain conformation, which precludes the formation of the C_β conformers.

Our studies based on combined theoretical vibrational spectra calculations of single chain fluorene oligomers and experimental Raman scattering studies of PF8 as a function of thermal cycling are an important step towards developing a universal picture of structure-property relationship in CPs that mainly derive from chain morphology at short length scales.

ACKNOWLEDGMENTS

We gratefully acknowledge the support of this work through the National Science Foundation under Grant No. ECS-0523656. One of us (S.G.) has greatly benefitted from fruitful discussions with Michael Winokur (MW). We also thank MW for the *p*-xylene cast PF8 sample.

[1] M. Leclerc, J. Polym. Sci. A **39**, 2867 (2001).
[2] D. Neher, Macromol. Rapid Commun. **22**, 1366 (2001).
[3] U. Scherf and E. J. W. List, Adv. Mater. (Weinheim, Ger.) **14**, 477 (2002).
[4] M. Grell, D. D. C. Bradley, G. Ungar, J. Hill, and K. S. Whitehead, Macromolecules **32**, 5810 (1999).
[5] A. J. Cadby, P. A. Lane, H. Mellor, S. J. Martin, M. Grell, C. Giebeler, D. D. C. Bradley, M. Wohlgenannt, C. An, and Z. V. Vardeny, Phys. Rev. B **62**, 15604 (2000).
[6] G. Lieser, M. Oda, T. Miteva, A. Meisel, H. G. Nothofer, and U. Scher, Macromolecules **33**, 4490 (2000).
[7] B. Tanto, S. Guha, C. M. Martin, U. Scherf, and M. J. Winokur, Macromolecules **37**, 9438 (2004).
[8] M. Knaapila, B. P. Lyons, K. Kisko *et al.*, J. Phys. Chem. B **107**, 12425 (2003).
[9] M. Knaapila, R. Stepanyan, M. Torkkeli *et al.*, Phys. Rev. E **71**, 041802 (2005).
[10] S. H. Chen, H. L. Chou, A. C. Su, and S. Chen, Macromolecules **37**, 6833 (2004).
[11] S. H. Chen, A. C. Su, C. H. Su, and S. A. Chen, Macromolecules **38**, 379 (2005).
[12] A. L. T. Khan, P. Sreearunothai, L. M. Herz, M. J. Banach, and A. Köhler, Phys. Rev. B **69**, 085201 (2004).
[13] M. J. Winokur, J. Slinker, and D. L. Huber, Phys. Rev. B **67**, 184106 (2003).
[14] W. Chunwaschirasiri, B. Tanto, D. L. Huber, and M. J. Winokur, Phys. Rev. Lett. **94**, 107402 (2005).
[15] M. Ariu, D. G. Lidzey, M. Sims, A. J. Cadby, P. A. Lane, and D. D. C. Bradley, J. Phys.: Condens. Matter **14**, 9975 (2002).
[16] M. Arif, C. Volz, and S. Guha, Phys. Rev. Lett. **96**, 025503 (2006).
[17] G. Zerbi, R. Magni, M. Gussoni, K. H. Mortiz, A. Bigotto, and S. Dirlikov, J. Chem. Phys. **75**, 3175 (1981).
[18] R. G. Snyder, J. Chem. Phys. **76**, 3921 (1982).
[19] Y. Kim, H. L. Strauss, and R. G. Snyder, J. Phys. Chem. **93**, 7520 (1989).
[20] L. Brambilla and G. Zerbi, Macromolecules **38**, 3327 (2005).
[21] M. Maroncelli, S. P. Qi, H. L. Strauss, and R. G. Snyder, J. Am. Chem. Soc. **104**, 6237 (1982).
[22] K. Ohno, H. Yoshida, H. Watanabe, T. Fujita, and H. Matsuura, J. Phys. Chem. **98**, 6924 (1994).
[23] R. F. Schaufele and T. Shimanouchi, J. Chem. Phys. **47**, 3605 (1967).
[24] GAUSSIAN03, Gaussian, Inc., Pittsburgh, PA, 2003.
[25] A. D. Becke, J. Chem. Phys. **98**, 5648 (1993).
[26] D. Porezag and M. R. Pederson, Phys. Rev. B **54**, 7830 (1996).
[27] R. E. Oakes, S. E. J. Bell, Z. Benkova, and A. J. Sadlej, J. Comput. Chem. **26**, 154 (2005).
[28] S. Guha, W. Graupner, R. Resel, M. Chandrasekhar, H. R. Chandrasekhar, R. Glaser, and G. Leising, J. Phys. Chem. A **105**, 6203 (2001).
[29] M. J. Frisch, Y. Yamaguchi, J. F. Gaw, H. F. Schaefer III, and J. S. Binkley, J. Chem. Phys. **84**, 531 (1986).
[30] L. Cuff and M. Kertesz, J. Phys. Chem. **98**, 12223 (1994).
[31] S. Irle and H. J. Lischka, J. Mol. Struct. **15**, 364 (1996).
[32] H. Liem, P. Etchegoin, K. S. Whitehead, and D. D. C. Bradley, J. Appl. Phys. **92**, 1154 (2002).
[33] M. Ariu, M. Sims, M. D. Rahn, J. Hill, A. M. Fox, D. G. Lidzey, M. Oda, J. Cabanillas-Gonzalez, and D. D. C. Bradley, Phys. Rev. B **67**, 195333 (2003).
[34] H. Cheun, B. Tanto, W. Chunwaschirasiri, B. Larson, and M. J. Winokur, Appl. Phys. Lett. **84**, 22 (2004).
[35] B. Tanto, S. Guha, M. Arif, and M. J. Winokur (unpublished).
[36] F. Negri and M. Z. Zgierski, J. Chem. Phys. **97**, 7124 (1992).